Avian-restrict *Salmonella* transition to endemicity is accompanied by localized resistome adaptation

Chenghao Jia[1], Chenghu Huang[1,2], Haiyang Zhou[1,2], Xiao Zhou[5], Zining Wang[1,2], Abubakar Siddique[1,2], Xiamei Kang[1], Qianzhe Cao[1], Yingying Huang[1,2], Fang He [1,6], Yan Li [1,2], Min Yue [1,2,3,4#]

[1] Department of Veterinary Medicine, Zhejiang University College of Animal Sciences, Hangzhou 310058, China
[2] Hainan Institute of Zhejiang University, Sanya 572000, China
[3] School of Life Science, Hangzhou Institute for Advanced Study, University of Chinese Academy of Sciences, Hangzhou 310024, China.
[4] State Key Laboratory for Diagnosis and Treatment of Infectious Diseases, National Clinical Research Center for Infectious Diseases, National Medical Center for Infectious Diseases, The First Affiliated Hospital, College of Medicine, Zhejiang University, Hangzhou 310003, China
[5] Ningbo Academy of Agricultural Sciences, Ningbo 315040, China
[6] ZJU-Xinchang Joint Innovation Centre (TianMu Laboratory), Gaochuang Hi-Tech Park, Zhejiang, China

Email address:
CJ: 22017118@zju.edu.cn
CH: 22217106@zju.edu.cn
ZH: zhouhaiyang@zju.edu.cn
XZ: xiaozhou_2023@163.com
ZW: znwang@zju.edu.cn
AS：abubakars@zju.edu.cn
XK: 12017032@zju.edu.cn
QC: 22317128@zju.edu.cn
YH: 22317127@zju.edu.cn
FH: hefangzj@zju.edu.cn
YL: yanli3@zju.edu.cn

Corresponding author:

Min Yue. Tel: +86 0571 88982832; E-mail: myue@zju.edu.cn

Abstract:

Bacterial regional demonstration after global dissemination is an essential pathway for selecting distinct finesses. However, the stepwise evolution of the resistome during the transition to endemicity remains unaddressed. Using the most comprehensive whole-genome sequencing dataset of *Salmonella* enterica serovar Gallinarum (*S*. Gallinarum) collected from 16 countries over the past century, we first elucidated the pathogen's population structure. Subsequently, we revealed the international transmission and evolutionary history of *S*. Gallinarum to recent endemicity through phylogenetic analysis conducted within a spatiotemporal Bayesian framework. Our findings indicate that the independent acquisition of the resistome via the mobilome, primarily through plasmids, transposons, and prophages, shapes a unique antimicrobial resistance profile. By utilizing the pipeline we developed to investigate the frequency of horizontal resistome transfer, we identified a significantly higher rate of cross-region dissemination compared to localized propagation, highlighting the key role of the resistome in driving the transition and evolutionary history of *S*. Gallinarum. Collectively, this study elucidates resistome adaptation in the endemic transition of a single pathogen, providing valuable insights for targeted policy interventions.

Keywords:

Salmonella; Mobilome; Resistome; Whole genome sequencing; Horizontal gene transfer

Introduction

The acquisition of antimicrobial resistance (AMR) by pathogens is well-established as one of the most serious threats of the 21st century (1–3). It is estimated that over 10 million people could die per year due to AMR by 2050 (4). Antimicrobial resistance genes (ARGs), collectively known as the resistome, play a pivotal role in AMR development, progression, and amplification (5). Pathogens typically acquire resistome through mobilomes, like plasmids, via horizontal gene transfer (HGT) (6, 7). From an evolutionary perspective, the dynamic change in the resistome is crucial for enhancing pathogen fitness and enabling it to colonize new ecological niches (8). Key factors contributing to resistome alterations include targeted human interventions, climate change, and geographical selection forces (9, 10). Understanding the evolutionary trajectory of the AMR and related reservoirs is necessary, as disease management strategies will differ substantially (11). However, knowledge regarding the overall profile of pathogen regional adaptation related to the stepwise dynamics of the resistome remains limited.

Before recent advancements in whole-genome sequencing (WGS) technology, little was understood about resistome diversity that affects pathogen endemicity (12). Traditional typing methods generally exhibit low resolution, making monitoring and quantitatively comparing horizontal ARG transfer events challenging. The scarcity of appropriate models also poses a limitation. *Salmonella*, a pathogen with strong geographical-related characteristics, has more than 90% serovars, frequently categorized as geo-serotypes (13). Among a few thousand geo-serotypes, *Salmonella* enterica serovar Gallinarum (*S.* Gallinarum) is an avian-specific agent, leading to horrific mortality rates that remain a disproportionate burden to the poultry industry in low- and middle-income countries (14, 15). As once a globally prevalent pathogen in the

20th century, *S.* Gallinarum was listed by the World Organization for Animal Health (WOAH) and gradually became an endemic pathogen with sporadic outbreaks following the implementation of eradication programs in most high-income countries, making it a perfect model for study (16, 17).

Nowadays, antimicrobial therapy is still used against *S.* Gallinarum infection (18). The overuse or misuse of antimicrobials has led to increased epidemiological escalation of *S.* Gallinarum, with a regionally higher risk of AMR, especially for sulfonamides, penicillin, and tetracyclines (19, 20). To fill the gaps in understanding the evolution of *S.* Gallinarum under regional-associated AMR pressures and its adaptation to endemicity, we collected the most comprehensive set of 580 *S.* Gallinarum isolates, covering the period from 1920 to 2023. Using WGS dataset we investigated: 1) the population structure and geographical transmission history of *S.* Gallinarum at a single base level; 2) the dynamic resistome and mobilome changes that are associated with *S.* Gallinarum transition to an endemic variant; and 3) horizontal resistome transfer frequency and pattern between distinct regions.

Results

Global distribution of *S.* Gallinarum links with distinct sublineages

To understand the global geographic distribution and genetic relationship of *S.* Gallinarum, we assembled the most comprehensive *S.* Gallinarum WGS dataset (n=580). The core genome SNPs (cgSNPs) were obtained by using the fully sequenced genome of *S.* Gallinarum R51 as a reference. Recombination regions in the genome were eliminated, and through hierarchical Bayesian analysis of cgSNPs, it was confirmed that *S.* Gallinarum divides into three biovars: bvSP (n=528/580, 91.03%), bvSG (n=50/580, 8.6%), and bvSD (n=2/580, 0.34%). An association was identified between the biovar type of *S.*

Gallinarum and its global geographic distribution. Most bvSP isolates were from Asia (436/528), with fewer occurrences in Europe (54/528), South America (12/528), and North America (5/528). In bvSG, South America (18/50, 36%) is the primary source of isolates, followed by North America (9/50, 18%), Europe (9/50, 18%), Africa (7/50, 14%), and Asia (3/50, 6%) (S1 Fig).

From a lineage perspective, bvSP can be further classified into five lineages: L1 (10/528), L2a (45/528), L2b (163/528), L3b (141/528), and L3c (169/528). Importantly, L3a, previously considered distinct, has been revealed as a sub-lineage of L3b. The predominant lineage types vary across different continents. Regarding predominant bvSP sources, Asia stands out, with L3c, L3b, and L2b being the main lineage types. On the other hand, L3c and L2a are more widespread in Europe and America, respectively (Fig 1a). Notably, all bvSP isolates from Asia were exclusively found in China, which can be manually divided into three distinct regions (southern, eastern, and northern). Our findings indicate significant variations in bvSP across various regions from geo-temporal aspects. Prevalence was highest in the eastern region (233/436), with lower incidences in the northern (137/436) and southern regions (65/436). Interestingly, the predominant bvSP lineage type also varied. In eastern and southern China, L2b and L3b emerged as the predominant lineage types, while in northern China, L3b and L3c held nearly equivalent positions (Fig 1c).

An analysis of the temporal prevalence of bvSP in China revealed a gradual replacement pattern of the lineages. Before the 2000s, the predominant lineage type was L3c. Then, from the 2000s to the 2010s, L3c and L1 were continually replaced by L3b, with L2b becoming the predominant lineage after the 2010s (Fig 1b). However, the replacement pattern varied among different regions. Specifically, the same pattern was observed in eastern China, but for northern

and southern China, only replacements from L3c to L2b and L1 to L3b were observed (S2 Fig). These findings might indicate accelerated localized adaptation of bvSP.

Genomics portrait bvSP historic transmission

Considering the historical pandemic status of bvSP, we then investigated its global geographic transmission routes to understand its evolution into an endemic pathogen. L2b and L3c were selected as the dominant global lineage types, and a Bayesian model with a relaxed molecular clock was used to infer the evolutionary dynamics and historical transmission routes using the BEAST software (Fig 2). The temporal structure was verified (S3 Fig), and our findings show that L2b emerged in China earlier than L3c, with potential spread from China to Europe as early as around the year 1800. Then, a long period of L2b spread internationally between South America and Europe was observed between 1800 and 1980. Notably, the L2b exhibited a return transmission from Europe to China around 1980, coinciding with the normalization of China-EU relations, as well as the timing of increased economic cooperation between China and Europe. In contrast, the historical transmission route for the L3c branch is more distinct, with L3c introduced to Europe from China around 1890 and reintroduced to China around 1910 (S4 Fig).

Endemic isolates further support localized dissemination pattern of bvSP

To investigate the dissemination pattern of bvSP in China, we obtained forty-five newly isolated bvSP from 734 samples (6.1% overall isolation rate) collected from diseased chickens at two farms in Yueqing and Taishun, Zhejiang Province. Those bvSP can be classified into two dominant sequence types (STs): ST3717 and ST92. Isolates from Yueqing were all identified as ST3717, while most Taishun isolates were characterized as ST92. Only the

E404 isolate was identified as ST2151 (Fig 3a). Interestingly, a lineage-preferential distribution was also observed, with bvSP isolated from Taishun belonging to L3c and those from Yueqing belonging to L2b. To further understand the genetic relationship among isolates in the two regions, we calculated cgSNPs distances between isolates. Isolates with cgSNP distances less than 100 were determined as the threshold to be involved in the same transmission event. Interestingly, genetic clustering revealed that isolates from the same farm exhibited a significantly close genetic correlation (Fig 3b). No historical transmission events of bvSP were found between Taishun and Yueqing.

Other genetic characteristics also exhibited a similar pattern. The ARG and plasmid profile disclosed that *IncFII(S)* and *ColpVC* plasmids exhibited the highest carriage percentages (100%) among the 45 bvSP isolates. The *IncX1* plasmid was exclusively identified in the E404 isolate. Furthermore, E404 harboured two distinctive resistance genes, $bla_{\text{TEM-1B}}$ and *sul2*, in contrast to the absence of ARGs in the remaining bvSP isolates. We also estimated the invasiveness index to assess the invasiveness of isolated bvSP and showed that bvSP from the same farm had comparable invasive abilities. However, isolates from Taishun demonstrated a higher invasive ability than those from Yueqing (Fig 3c).

Furthermore, we simulated potential transmission events between the bvSP strains isolated from Zhejiang Province and those from other provinces of China. As a result, the transmission events showed a strong geographic-preferential distribution. The number of transmission events decreased quickly with increasing distance, which provides additional support for bvSP in China belonging to a highly localized pathogen (S5 Fig).

Mobilome and resistome distinct lineage-preferential distribution in a regional manner

The mobilome drives partitions of the resistome and plays a pivotal role in shaping the ecological niches of bacteria. Therefore, a quantitative evaluation of the resistome and mobilome is necessary to enhance the understanding of the localized distribution of bvSP. For *S.* Gallinarum, a total of 13 classes of ARGs, which can be further classified into six categories, were identified. The results revealed that bvSP exhibited a significantly greater resistome than bvSG and bvSD (Fig 4a). Among them, *sul2* (196/528, 37.1%) has the highest prevalence, followed by $bla_{\text{TEM-1B}}$ (183/528, 34.7%) and *tet(A)* (104/528, 19.7%). Moreover, the resistome also demonstrated a lineage-preferential distribution. We observed that L3b is more inclined to carry $bla_{\text{TEM-1B}}$ and *sul2* than other lineages, whereas *tet(A)* exclusively exists within L3. The diversity of resistome carried by L3 may elevate the risk of multi-drug resistance (MDR). Notably, AMR risks vary among different regions of China, with the highest risk observed in southern China, followed by the northern and eastern regions (Fig 4c). Interestingly, *tet(A)*, $bla_{\text{TEM-1B}}$, and *sul2* were predominant resistome types prevalent across all regions of China. Meanwhile, *aadA5* was typically more commonly found in southern China (Fig 4b).

Four categories of the mobilome—prophage, plasmid, transposon, and integron—were characterized, revealing strong lineage-specific patterns (S6a Fig). In silico analyses revealed prophages emerge as the most diverse mobilome type, with *Entero_mEp237*, *Escher_500465_1, and Klebsi_4LV2017* being more likely associated with L1, L2a, and L2b, respectively, while the carrier percentage of *Escher_pro483* is significantly higher among L3b. Interestingly, *Salmon_SJ46, Gifsy_2*, *Escher_500465_2,* and *Shigel_SfIV*

were consistently observed across all bvSP lineages and were found to be duplicated on the chromosome. For plasmids, *IncFII(S)* was predominantly carried across all bvSP lineages (520/528, 98.5%) (S6b Fig). Notably, *ColpVC* had the lowest carriage percentage among L1 (2/10, 20%), whereas *IncX1* was explicitly associated with L3b (140/141, 99.3%).

The diversity of transposons and integrons is comparatively lower in bvSP. Specifically, we identified seven types of transposons and four types of integrons. Transposons were found to be more abundant, comprising a total of 255 in 528 bvSP. Among them, *Tn801* (185/528, 35%) had the highest carriage rate, followed by *Tn1721* (48/528, 9.1%). Interestingly, L3b is more likely to carry *Tn801* and *Tn1721* transposons than other lineages. In contrast, a total of 42 integrons were identified among the 528 bvSP, all of which belong to class I: *In498* (n=22), *In1440* (n=14), *In473* (n=4), and *In282* (n=2). The integrons also exhibited a lineage-preferential distribution, predominantly carried by L3c. From a geographic distribution perspective, bvSP from northern and southern China carried the most extensive mobilome, followed by those from eastern China. Interestingly, bvSP isolated from northern China typically have a greater variety of mobilome types (S7 Fig).

Plasmids and transposons guide resistome geo-temporal dissemination

Variations in regional antimicrobial use result in an uneven distribution of AMR risks. The mobilome is considered the primary reservoir for spreading resistome, and a consistent trend between the resistome and the mobilome has been observed across different lineages, from L1-L3c. We observed an overall gradual rise in the resistome quantity carried by bvSP across various lineages, correlating with the total mobilome content (S8 Fig). In more detail, both the resistome and mobilome exhibited a steady decline until the 1980s, followed by

a consistent increase from the 1980s to the 2010s. However, after the 2010s, a subsequent decrease was identified. Consequently, we further investigated the interplay between mobilome and resistome in bvSP.

In bvSP, the predominant resistome is carried by the mobilome (Fig 5a). Specifically, regarding *bla*$_{TEM_1B}$, *tet(A)*, and *sul1*, which are highly prevalent among bvSP, we found most *bla*$_{TEM_1B}$ were carried by the transposon *Tn801* and *Tn1721*, the plasmid *IncX1*, and the prophage SJ46. Additionally, *tet(A)* was primarily associated with the transposon *Tn1721* and the plasmid IncX1. Integrons also facilitated the dissemination of the resistome. For instance, *In498* and *In1440* facilitate the dissemination of *sul1*, leading to quinolone resistance. Our results indicate that plasmids and transposons serve as the predominant reservoirs for the resistome in bvSP, with prophages and integrons following closely behind (Fig 5b). Interestingly, we observed that the primary reservoir for the resistome shows regional variations. In the southern and northern regions of China, the primary reservoirs for *bla*$_{TEM_1B}$ are *Tn801*, *Tn1721*, *IncX1*, and prophage SJ46. However, *Tn1721* was less frequently found in bvSP, which carries *bla*$_{TEM\text{-}1B}$ from the eastern region. Similarly, the reservoir for *tet(A)* exhibits greater diversity in the east region but less diversity in the southern region (Fig 5c-e).

Horizontal transfer of resistome occurs widely in localized bvSP

Horizontal transfer of the resistome facilitates the acquisition of AMR among bacteria. Subsequently, we further investigated the HGT frequency of each ARG carried by bvSP isolated from China and explored the HGT frequency of resistome between various regions. Horizontal transfer of ARGs is defined as sequences with perfect identity (100% identity and 100% coverage) (Fig. 6a). Our findings indicate that horizontal transfer of the ARGs is widespread among

Chinese isolates of bvSP. Specifically, 60% of the ARGs exhibited an HGT frequency of 100%, indicating that these ARGs had undergone horizontal transfer at least once (Fig. 6b). It is noteworthy that certain resistance genes, such as *tet(A)*, *aph(3'')-Ib*, and *aph(6)-Id*, appear to be less susceptible to horizontal transfer.

However, different regions generally exhibited non-uniform resistome HGT frequency. Overall, bvSP from the southern region of China exhibited the highest HGT frequency (HGT frequency=97%). The HGT frequencies for bvSP within the eastern and northern regions of China are lower, at 91% and 90%, respectively (Fig. 6c). For specifically ARG type, we found *tet(A)* is more prone to horizontal transfer in the southern region, and this proportion was considerably lower in the eastern region. Interestingly, certain ARGs such as $bla_{\text{TEM-116}}$ only undergo horizontal transfer within a single region of eastern China (Fig. 6d). Notably, as a localized transmission pathogen, resistome carried by bvSP exhibited a strong risk of cross-regional transmission, especially from northern region to southern region (HGT frequency=95%) (Fig. 6e).

Discussion

Over the past decades, the emergence of AMR has garnered significant attention from both public health agencies and the poultry industry (21). Region-associated pressures shaped the dissemination patterns of bacterial pathogens, transitioning from pandemic to endemic, and led to dynamic changes in the resistome. Here, utilizing *S.* Gallinarum as a prototype for an endemic pathogen that once spread globally, and assembling the most comprehensive *S.* Gallinarum WGS database, we have discovered that region-associated pressures can influence the AMR risks of *S.* Gallinarum

within lineage- and region-specific patterns. These pressures might also influence lineage-distinct evolutionary structures and transmission histories of *S.* Gallinarum.

The biovar types of *S.* Gallinarum have been well-defined as bvSP, bvSG, and bvSD historically (22). Among these, bvSP can be further subdivided into five lineages (L1, L2a, L2b, L3b, and L3c) using hierarchical Bayesian analysis. Different sublineages exhibited preferential geographic distribution, with L2b and L3c of bvSP being predominant global lineage types. The historical geographical transmission was verified using a spatiotemporal Bayesian framework. The result shows that both lineages were initially spread from China to Europe in the early 19th century, which correlates strongly with the European hen fever event in the mid-19th century (23). Subsequently, the practice of breeding Asian chickens gradually spread from Europe to South America, leading to the bvSP prevalence in the United States. Considering the economic losses caused by bvSP, the United States, Europe, and other major countries implemented eradication programs in the mid-19th century, thus eliminating the risk of pullorum disease. However, with the strengthening of China-EU relations in the 1980s, a transmission of L2b from Europe to China was observed. Implementing similar measures is challenging due to China's vast geographical area and various economic factors, resulting in bvSP becoming an endemic pathogen, mainly in China.

Additionally, forty-five bvSP was isolated from Taishun and Yueqing, to explore the transmission pattern of bvSP in China. The cgSNP distances between bvSP isolates from Taishun and Yueqing, showed significant diversity, with cgSNP distances of less than 100 isolate pairs observed exclusively within a single region. The transmission history of 45 global bvSP isolates

revealed that most transmission events occurred within a single region. Additionally, the number of transmission events decreased rapidly with increasing distance, confirming that bvSP in China belongs to a highly localized pathogen.

Humanity appeared powerless against epidemics until the advent of antimicrobials, which are still the primary agents used to combat *S.* Gallinarum infection (24, 25). As a manifestation of localization-related forces, the emergence of AMR allows pathogens to acquire additional fitness benefits (26). Our findings further indicate that the mobilome facilitates the acquisition of AMR among bvSP, mainly through plasmids and transposons, such as *IncX1*, *IncQ1*, and *IncN* type plasmids, as well as *Tn801*, *Tn6205*, and *Tn721* type transposons. A survey conducted in China between 1962 and 2010 documented the association of class 1 integrons with AMR among bvSP (27). Our study further demonstrates that *In498*, *In1440*, *In473*, and *In282*, all belonging to class 1 integrons, play a significant role in carrying ARGs associated with sulfonamides, and trimethoprim. However, compared to other *Salmonella* serovars (28–30), the level of resistome in bvSP remains lower.

Considering lineage prospects, recently emerged lineages present a higher risk of AMR, with a lineage-specific distribution of resistome. In L2b and L3b, the most prevalent groups of ARGs include $bla_{\text{TEM-1b}}$ and *sul2*. L3c, which exhibits the highest resistome richness with *sul1*, *tet(A)*, *aadA5*, and *dfrA17*, has a higher likelihood of MDR. However, the transmission routes of resistome showed a high degree of consistency across continents. Globally, a small proportion of resistome carriers belonging to L2b and L3c were observed in the Americas and Europe, while isolates from Asia exhibited a notable rise in resistome carriage. Therefore, we speculate that the mobilome in bvSP may

have been acquired locally in Asia, possibly due to increased antimicrobial usage and an intensive industrialized poultry farming pattern within the regional poultry industry (31). The L3b, being a local Asian lineage and more prone to acquiring additional resistome locally, provided further support.

In China, the endemic region of Asia, an unexpected rising trend has been observed from the 1970s to the 2020s. However, the risk of AMR varies among distinct regions. Overall, the average number of ARGs carried by bvSP isolated from eastern China was the lowest, while it was higher among bvSP isolated from northern and southern China. This variation may be influenced by differences in the economy, climate, or farming practices among different regions. Interestingly, the widespread horizontal transfer of the resistome across regions seems to indicate that the resistome has a different mode of transmission compared to its host. Specifically, as a localized pathogen, our results show a low frequency of cross-regional transmission of bvSP (as shown in S5 Fig), but up to 90% of ARGs are transmitted cross-regionally. This risk has not been previously observed in *S.* Gallinarum, suggesting that potential intermediate hosts may play a key role.

However, the current study has some limitations. Firstly, despite assembling the most comprehensive WGS database for *S.* Gallinarum from public and laboratory sources, there are still biases in the examined collection. The majority (438/580) of *S.* Gallinarum samples were collected from China, possibly since the WGS is a technology that only became widely available in the 21st century. This makes it impractical to sequence it on a large scale in the 20th century, when *S.* Gallinarum caused a global pandemic. So, we suspect that human intervention in the development of this epidemic is the main driving force behind the fact that most of the strains in the data set

originated in China. Secondly, in silico analysis relies heavily on sophisticated, continuously updated databases. Although we utilized the most up-to-date databases, the exact prevalence of MGEs and ARGs may be underestimated. Nevertheless, by using the most extensive global WGS data from *S.* Gallinarum, we elucidate a dynamic resistome evolution framework in a single bacterial pathogen from pandemic to endemic, which is hallmarked by a gradual increase in antimicrobial resistance risks and a stepwise resistome adaptation. The insights gained in this study will be helpful in further prevention and surveillance of the AMR risks of localized pathogens.

Material and Methods

Ethics statements

The protocols used for animal studies were approved by the Committee of the Laboratory Animal Center of Zhejiang University (ZJU20190094; ZJU20220295).

Bacterial isolates

All 734 samples of dead chicken embryos were collected from Taishun and Yueqing in Zhejiang Province, China. After a thorough autopsy, the liver, intestines, and spleen were extracted and added separately into 2 mL centrifuge tubes containing 1 mL PBS. The organs were then homogenized by grinding. In the initial enrichment phase, we utilized Buffered Peptone Water (BPW, Haibo Biotechnology Co, Qingdao, China), employing a 1:9 dilution ratio (sample in PBS: BPW). Subsequently, the composite was incubated at 37°C for 16-18 hours in a rotary incubator set to 180 rpm. For selective enrichment, Tetrathionate Broth Base (TTB, Land Bridge Biotechnology Co, Beijing, China), fortified with iodine solution and brilliant green solution (both from Land Bridge

Biotechnology Co, Beijing, China), was employed at a ratio of 1:10 (sample in BPW: TTB). The mixture was subjected to incubation at 42°C for a duration ranging between 22 and 26 hours within a rotary incubator set at 180 rpm. Isolated *Salmonella* colonies from positive samples were obtained by sub-culturing selectively enriched samples on Xylose Lysine Deoxycholate (XLD, Land Bridge Technology Co, Beijing, China) agar, followed by an 18–22-hour incubation at 37°C. Typical and pure colonies were selected after sub-culturing on XLD agar and transferred into Luria-Bertani (LB) broth. Finally, the transferred bacterial culture underwent an additional incubation for 18-22 hours at 37°C in a rotary incubator operating at 180 rpm.

DNA extraction and genomic assembly

The DNA of forty-five isolates was extracted using the Vazyme Fastpure® Bacteria DNA Isolation Mini Kit (Vazyme Biotech Co., Ltd.), which was then quantified using the NanoDrop1000 system (Thermo Fisher Scientific, USA). Subsequently, DNA libraries were constructed and subjected to sequencing using the Illumina Novaseq 6000 platform (Novogene, Beijing, China). Assembly of genome sequences was performed by SPAdes (32) v3.12.0 with default parameters.

Global dataset assembly

To provide global context, we expanded the dataset by including 540 additional WGS genome data, consisting of bvSP (n=483), bvSG (n=50), bvSD (n=2), and *Salmonella* serovar Enteritidis (n=5). The inclusion of five strains of *Salmonella* enterica serovar Enteritidis enhanced evolutionary analyses. Notably, in this collection of 540 genomic data from public databases, 325 sequences were previously preserved in our laboratory.

All WGS data passed strict quality control according to criteria set by the European Reference Laboratory (33). Genomic data exceeding 500 contigs and having an N50 of less than 30,000 were excluded. Moreover, we considered GC content within the range of 51% to 53%. Lastly, the bacterial species associated with each genomic data set was confirmed by utilizing KmerFinder (34) v3.2. Finally, the assembled database includes a total of 585 high-quality sequences.

Genotyping and phylogenetic analyses

Snippy v.4.4.5 was used to identify cgSNPs, and Gubbins v.2.3 (35) was used to eliminate the recombination regions, with the complete genome of R51 used as a reference. The optimal model (TVM+F) was determined and employed to construct the maximum-likelihood phylogenetic tree using IQ-TREE v.1.6 (36). The final phylogenetic tree was annotated and visualized using iTOL v.6.0 (37).

The global assembly of *S.* Gallinarum underwent a population structure analysis using the RhierBAPS v1.1.4 (38), based on the Hierarchical Bayesian clustering (BHC) algorithm and employing cgSNPs as input. The calculation of population structure utilized R package v.4.3.1, supplemented by the R packages "phytools" v.2.0.3, "ape" v.5.7.1, and "rhierbaps" v.1.1.4. Default parameters were employed for all population structure analysis.

Temporal and phylogeographical analysis

To examine the emergence and geographical transfers, we first utilized TreeTime (39) to assess the temporal structure. This was accomplished through regression analysis of the root-to-tip branch distances within the maximum likelihood tree, considering the sampling date as a variable. Then, the strains within the dataset underwent phylogeographical reconstruction via

Bayesian Evolutionary Analysis of Sampled Trees (BEAST) (40) v.2.5. The BEAST analysis was performed on alignments of concatenated cgSNPs following previously described parameters (41). Maximum clade credibility trees were generated using TreeAnnotator v.2.6.7, and the tree was annotated and visualized using Figtree v.1.4.3.

To understand potential transmission events, we calculated the cgSNPs distance between distinct bacterial strains employing the SNP-dists, with cgSNPs distance less than 100 deemed indicatives of high similarity between two strains. Additionally, the geographic location and isolation date were considered to enhance the precision of speculation regarding potential transmission sites and the direction of transmission.

MGE detecting

Four types of MGEs were detected: plasmids, transposons, integrons, and prophages. Plasmids were detected using Abricate v.1.0.1 with the PlasmidFinder (42) database. Only plasmids with a similarity of more than 90% and a coverage over 95% were identified. BacAnt (43) was used to detect integrons and transposons in the genomes. Only integrons or transposons with a similarity of more than 60% and a coverage greater than 60% will be identified. The prophages were detected using the Phaster pipeline. The genomic data were split into two temporary databases based on the number of contigs, one dataset containing single contig files and the other containing multiple contig files. The two databases were imported into the Phaster pipeline separately with default parameters.

Determination of the potential MGE carried ARG and horizontal ARG transfer frequency

We have devised a pipeline to discern the coexistence of MGEs and ARGs. For plasmids and prophages, only ARGs situated within MGE regions are deemed MGE-carried. Regarding transposons and integrons, the search region was expanded to 5 kilobases upstream and downstream of ARGs, accounting for potential splicing errors. In this study, HGT events involving ARGs were defined as instances where ARGs exhibited perfect identity (100% coverage and 100% identity). In a previous study (44), horizontal transfer of ARGs was identified based on gene regions with 100% coverage and over 99% identity. We believe that these stricter criteria in our pipeline more accurately reflect the transfer of ARGs within the *S.* Gallinarum population. HGT frequency was utilized to evaluate the extent of horizontal transfer of ARGs as follows:

$$HGT\ frequency = \frac{\text{Horizontal ARG transfer Count}}{\text{Total dissemination count}}$$

The pipeline developed in this study accepts Resfinder or Resistance Gene Identifier (RGI) results as input. Specific code and examples are uploaded to: https://github.com/tjiaa/Cal_HGT_Frequency/tree/main.

Genomic data analysis

The serovars of all WGS genome data were confirmed through SISTR (45) v.1.1 and Seqsero2 (46). Multilocus Sequence Typing was carried out using MLST v.2.22 with the senterica_achtman_2 scheme. ARGs were detected by ResFinder (47). Both similarity and coverage were set to a minimum value of 90. The invasiveness index was calculated using methods previously reported (48). Briefly, we utilized the pre-trained random forest model along with R v4.1.2 to compute the invasiveness index. This approach demonstrated the feasibility of calculating the invasiveness index across various *Salmonella* species. Specifically, we adopted the DeltaBS metric to detect mutations in

protein-coding genes within the Whole Genome Sequence of the strains used for model training, resulting in the identification of 196 top predicted genes associated with invasiveness in *S.* enterica. The code used to calculate the invasiveness index is accessible at https://github.com/Gardner-BinfLab/invasive_salmonella.

Data Availability

The genome data of the newly isolated forty-five *S.* Gallinarum strains have been deposited into the China National GenBank Database (CNGBdb) under accession number CNP0005633. Additionally, the genome data for the 540 publicly available genomes have been uploaded to Figureshare and can be accessed at:
https://figshare.com/articles/journal_contribution/Genomic_data/26028592.

Code availability

The open-source software used in this study includes:
BacAnt (https://github.com/xthua/bacant),
Abricate (https://github.com/tseemann/abricate),
Snippy (https://github.com/tseemann/snippy),
SISTR (https://github.com/phac-nml/sistr_cmd),
MLST (https://cge.food.dtu.dk/services/MLST/)
SeqSero2 (https://github.com/denglab/SeqSero2),
IQtree (https://github.com/iqtree/iqtree2).
BEAST (https://www.beast2.org)
SNP-dists (https://github.com/tseemann/snp-dists)
Fast BAPS (https://github.com/gtonkinhill/fastbaps)
R (https://www.r-project.org)

Phaster (http://phaster.ca)

KmerFinder (https://bitbucket.org/genomicepidemiology/kmerfinder)

Treetime (https://github.com/neherlab/treetime)

Author contributions

M.Y., C.J. designed the study; finalized the manuscript;

C.J. collected isolates and clinical data, integrated the data, performed metadata and genomic analysis, prepared tables and figures; and wrote the draft manuscript;

C.H. performed metadata and genomic analysis; interpreted the data; finalized the manuscript;

X.Z., X.K., Q.C., Y.H. and Z.W. contributed to the data analysis;

C.H., M.Y. prepared tables and figures;

M.Y., C.H., A.S., Y.L., F.H., and C.J. finalized the manuscript;

M.Y. managed the project;

All the authors contributed to the article and approved the submitted version.

Declaration of Interests

None.

Acknowledgements

This work was supported by the National Program on the Key Research Project of China (2022YFC2604201), the Zhejiang Provincial Natural Science Foundation of China (LZ24C180002; LR19C180001), the Hainan Provincial Joint Project of Sanya Yazhou Bay Science and Technology City (2021JJLH0083), the Zhejiang Provincial Key R&D Program of China (2023C03045, 2022C02024) and the Open Project Program of the Jiangsu Key

Laboratory of Zoonosis (R1902), and the European Union's Horizon 2020 Research and Innovation Programme under Grant Agreement No. 861917 – SAFFI.

Reference

1. Li Y, Ed-Dra A, Tang B, Kang X, Müller A, Kehrenberg C, Jia C, Pan H, Yang H, Yue M. 2022. Higher tolerance of predominant Salmonella serovars circulating in the antibiotic-free feed farms to environmental stresses. Journal of Hazardous Materials 438:129476.

2. Hou J, Long X, Wang X, Li L, Mao D, Luo Y, Ren H. 2023. Global trend of antimicrobial resistance in common bacterial pathogens in response to antibiotic consumption. Journal of Hazardous Materials 442:130042.

3. Lee K, Raguideau S, Sirén K, Asnicar F, Cumbo F, Hildebrand F, Segata N, Cha C-J, Quince C. 2023. Population-level impacts of antibiotic usage on the human gut microbiome. Nat Commun 14:1191.

4. Rappuoli R, Bloom DE, Black S. 2017. Deploy vaccines to fight superbugs. Nature 552:165–167.

5. Larsson DGJ, Flach C-F. 2022. Antibiotic resistance in the environment. Nat Rev Microbiol 20:257–269.

6. Tóth AG, Judge MF, Nagy SÁ, Papp M, Solymosi N. 2023. A survey on antimicrobial resistance genes of frequently used probiotic bacteria, 1901 to 2022. Eurosurveillance 28.

7. Jia C, Wang Z, Huang C, Teng L, Zhou H, An H, Liao S, Liu Y, Huang L, Tang B, Yue M. 2023. Mobilome-driven partitions of the resistome in *Salmonella*. mSystems 8:e00883-23.

8. Carr VR, Witherden EA, Lee S, Shoaie S, Mullany P, Proctor GB, Gomez-Cabrero D, Moyes DL. 2020. Abundance and diversity of resistomes differ between healthy human oral cavities and gut. Nat Commun 11:693.

9. Jia C, Cao Q, Wang Z, Van Den Dool A, Yue M. 2024. Climate change affects the spread of typhoid pathogens. Microbial Biotechnology 17:e14417.

10. Petersen E, Petrosillo N, Koopmans M, Beeching N, Di Caro A, Gkrania-Klotsas E, Kantele A, Kohlmann R, Koopmans M, Lim P-L, Markotic A, López-Vélez R, Poirel L, Rossen JWA, Stienstra Y, Storgaard M. 2018. Emerging infections—an increasingly important topic: review by the Emerging Infections Task Force. Clinical Microbiology and Infection 24:369–375.

11. Baquero F, Martínez JL, F. Lanza V, Rodríguez-Beltrán J, Galán JC, San Millán A, Cantón R, Coque TM. 2021. Evolutionary Pathways and Trajectories in Antibiotic Resistance. Clin Microbiol Rev 34:e00050-19.

12. Didelot X, Bowden R, Wilson DJ, Peto TEA, Crook DW. 2012. Transforming clinical microbiology with bacterial genome sequencing. Nat Rev Genet 13:601–612.

13. Gossner CM, Le Hello S, De Jong B, Rolfhamre P, Faensen D, Weill F-X, Johan Giesecke. 2016. Around the World in 1,475 *Salmonella* Geo-serotypes. Emerg Infect Dis 22:1298–1302.

14. Kang X, Zhou X, Tang Y, Jiang Z, Chen J, Mohsin M, Yue M. 2022. Characterization of Two-Component System CitB Family in Salmonella Pullorum. IJMS 23:10201.

15. Zhou X, Kang X, Zhou K, Yue M. 2022. A global dataset for prevalence of Salmonella Gallinarum between 1945 and 2021. Sci Data 9:495.

16. Zhou X, Kang X, Chen J, Song Y, Jia C, Teng L, Tang Y, Jiang Z, Peng X, Tao X, Xu Y, Huang L, Xu X, Xu Y, Zhang T, Yu S, Gong J, Wang S, Liu Y, Zhu G, Kehrenberg C, Weill F-X, Barrow P, Li Y, Zhao G, Yue M. 2023. Genome degradation promotes *Salmonella* pathoadaptation by remodeling fimbriae-mediated proinflammatory response. National Science Review 10:nwad228.

17. De Carli S, Gräf T, Kipper D, Lehmann FKM, Zanetti N, Siqueira FM, Cibulski S, Fonseca ASK, Ikuta N, Lunge VR. 2017. Molecular and phylogenetic analyses of Salmonella Gallinarum trace the origin and diversification of recent outbreaks of fowl typhoid in poultry farms. Veterinary Microbiology 212:80–86.

18. Barrow PA, Neto OCF. 2011. Pullorum disease and fowl typhoid—new thoughts on old diseases: a review. Avian Pathology 40:1–13.

19. Nhung NT, Chansiripornchai N, Carrique-Mas JJ. 2017. Antimicrobial Resistance in Bacterial Poultry Pathogens: A Review. Front Vet Sci 4:126.

20. Penha Filho RAC, Ferreira JC, Kanashiro AMI, Darini AL da C, Berchieri Junior A. 2016. Antimicrobial susceptibility of Salmonella Gallinarum and Salmonella Pullorum isolated from ill poultry in Brazil. Ciência Rural 46:513–518.

21. Huang L, Zhou H, Chen J, Jia C, Siddique A, Wu B, Wang H, Tang B, He F, Zhao G, Yue M. 2024. Impact of COVID-19-related nonpharmaceutical interventions on diarrheal diseases and zoonotic Salmonella. hLife S294992832400021X.

22. Kisiela D, Kuczkowski M, Kiczak L, Wieliczko A, Ugorski M. 2005. Differentiation of *Salmonella* Gallinarum biovar Gallinarum from *Salmonella* Gallinarum biovar Pullorum by PCR-RFLP of the *fimH* gene. Journal of Veterinary Medicine, Series B 52:214–218.

23. Burnham GP. 1855. The history of the hen fever: a humorous record. James French.

24. Worboys M. 2000. Spreading germs: disease theories and medical practice in Britain, 1865-1900. Cambridge University Press.

25. Porter R, Crosby AW. 1998. The Greatest Benefit to Mankind: A Medical History of Humanity from Antiquity to the Present. Nature 391:241–241.

26. Helekal D, Keeling M, Grad YH, Didelot X. 2023. Estimating the fitness cost and benefit of antimicrobial resistance from pathogen genomic data. J R Soc Interface 20:20230074.

27. Gong J, Xu M, Zhu C, Miao J, Liu X, Xu B, Zhang J, Yu Y, Jia X. 2013. Antimicrobial resistance, presence of integrons and biofilm formation of *Salmonella* Pullorum isolates from eastern China (1962–2010). Avian Pathology 42:290–294.

28. Li Y, Teng L, Xu X, Li X, Peng X, Zhou X, Du J, Tang Y, Jiang Z, Wang Z, Jia C, Müller A, Kehrenberg C, Wang H, Wu B, Weill F, Yue M. 2022. A nontyphoidal *Salmonella* serovar domestication accompanying enhanced niche adaptation. EMBO Mol Med 14:e16366.

29. Teng L, Liao S, Zhou X, Jia C, Feng M, Pan H, Ma Z, Yue M. 2022. Prevalence and Genomic Investigation of Multidrug-Resistant Salmonella Isolates from Companion Animals in Hangzhou, China. Antibiotics 11:625.

30. Pan H, Jia C, Paudyal N, Li F, Mao J, Liu X, Dong C, Zhou K, Liao X, Gong J, Fang W, Li X, Kehrenberg C, Yue M. 2022. Comprehensive Assessment of Subtyping Methods for Improved Surveillance of Foodborne Salmonella. Microbiol Spectr 10:e02479-22.

31. Kumar D, Pornsukarom S, Thakur S. 2019. Antibiotic usage in poultry production and antimicrobial-resistant Salmonella in poultry. Food safety in poultry meat production 47–66.

32. Bankevich A, Nurk S, Antipov D, Gurevich AA, Dvorkin M, Kulikov AS, Lesin VM, Nikolenko SI, Pham S, Prjibelski AD, Pyshkin AV, Sirotkin AV, Vyahhi N, Tesler G, Alekseyev MA, Pevzner PA. 2012. SPAdes: A New Genome Assembly Algorithm and Its Applications to Single-Cell Sequencing. Journal of Computational Biology 19:455–477.

33. Ellington MJ, Ekelund O, Aarestrup FM, Canton R, Doumith M, Giske C, Grundman H, Hasman H, Holden MTG, Hopkins KL, Iredell J, Kahlmeter G, Köser CU, MacGowan A, Mevius D, Mulvey M, Naas T, Peto T, Rolain J-M, Samuelsen Ø, Woodford N. 2017. The role of whole genome sequencing in antimicrobial susceptibility testing of bacteria: report from the EUCAST Subcommittee. Clinical Microbiology and Infection 23:2–22.

34. Hasman H, Saputra D, Sicheritz-Ponten T, Lund O, Svendsen CA, Frimodt-Møller N, Aarestrup FM. 2014. Rapid Whole-Genome Sequencing for Detection and Characterization of Microorganisms Directly from Clinical Samples. J Clin Microbiol 52:139–146.

35. Croucher NJ, Page AJ, Connor TR, Delaney AJ, Keane JA, Bentley SD, Parkhill J, Harris SR. 2015. Rapid phylogenetic analysis of large samples of recombinant bacterial whole genome sequences using Gubbins. Nucleic Acids Research 43:e15–e15.

36. Nguyen L-T, Schmidt HA, Von Haeseler A, Minh BQ. 2015. IQ-TREE: A Fast and Effective Stochastic Algorithm for Estimating Maximum-Likelihood Phylogenies. Molecular Biology and Evolution 32:268–274.

37. Letunic I, Bork P. 2021. Interactive Tree Of Life (iTOL) v5: an online tool for phylogenetic tree display and annotation. Nucleic Acids Research 49:W293–W296.

38. Cheng L, Connor TR, Siren J, Aanensen DM, Corander J. 2013. Hierarchical and Spatially Explicit Clustering of DNA Sequences with BAPS Software. Molecular Biology and Evolution 30:1224–1228.

39. Sagulenko P, Puller V, Neher RA. 2018. TreeTime: Maximum-likelihood phylodynamic analysis. Virus Evolution 4.

40. Bouckaert R, Vaughan TG, Barido-Sottani J, Duchêne S, Fourment M, Gavryushkina A, Heled J, Jones G, Kühnert D, De Maio N, Matschiner M, Mendes FK, Müller NF, Ogilvie HA, Du Plessis L, Popinga A, Rambaut A, Rasmussen D, Siveroni I, Suchard MA, Wu C-H, Xie D, Zhang C, Stadler T, Drummond AJ. 2019. BEAST 2.5: An advanced software platform for Bayesian evolutionary analysis. PLoS Comput Biol 15:e1006650.

41. Feng Y, Pan H, Zheng B, Li F, Teng L, Jiang Z, Feng M, Zhou X, Peng X, Xu X, Wang H, Wu B, Xiao Y, Baker S, Zhao G, Yue M. 2023. An integrated nationwide genomics study reveals transmission modes of typhoid fever in China. mBio 14:e01333-23.

42. Carattoli A, Zankari E, García-Fernández A, Voldby Larsen M, Lund O, Villa L, Møller Aarestrup F, Hasman H. 2014. *In Silico* Detection and

Typing of Plasmids using PlasmidFinder and Plasmid Multilocus Sequence Typing. Antimicrob Agents Chemother 58:3895–3903.

43. Hua X, Liang Q, Deng M, He J, Wang M, Hong W, Wu J, Lu B, Leptihn S, Yu Y, Chen H. 2021. BacAnt: A Combination Annotation Server for Bacterial DNA Sequences to Identify Antibiotic Resistance Genes, Integrons, and Transposable Elements. Front Microbiol 12:649969.

44. Wang X, Zhang H, Yu S, Li D, Gillings MR, Ren H, Mao D, Guo J, Luo Y. 2024. Inter-plasmid transfer of antibiotic resistance genes accelerates antibiotic resistance in bacterial pathogens. The ISME Journal 18:wrad032.

45. Yoshida CE, Kruczkiewicz P, Laing CR, Lingohr EJ, Gannon VPJ, Nash JHE, Taboada EN. 2016. The Salmonella In Silico Typing Resource (SISTR): An Open Web-Accessible Tool for Rapidly Typing and Subtyping Draft Salmonella Genome Assemblies. PLoS ONE 11:e0147101.

46. Zhang S, Den Bakker HC, Li S, Chen J, Dinsmore BA, Lane C, Lauer AC, Fields PI, Deng X. 2019. SeqSero2: Rapid and Improved *Salmonella* Serotype Determination Using Whole-Genome Sequencing Data. Appl Environ Microbiol 85:e01746-19.

47. Zankari E, Hasman H, Cosentino S, Vestergaard M, Rasmussen S, Lund O, Aarestrup FM, Larsen MV. 2012. Identification of acquired antimicrobial resistance genes. Journal of Antimicrobial Chemotherapy 67:2640–2644.

48. Van Puyvelde S, Pickard D, Vandelannoote K, Heinz E, Barbé B, De Block T, Clare S, Coomber EL, Harcourt K, Sridhar S, Lees EA, Wheeler NE, Klemm EJ, Kuijpers L, Mbuyi Kalonji L, Phoba M-F, Falay D, Ngbonda D, Lunguya O, Jacobs J, Dougan G, Deborggraeve S. 2019. An African

Salmonella Typhimurium ST313 sublineage with extensive drug-resistance and signatures of host adaptation. Nat Commun 10:4280.

Figure Legends

Figure 1. Genetic diversity of bvSP by geography and time. Different colours were used to represent the various lineages of bvSP: fuchsia for L1, orange for L2a, pink for L2b, green for L3b, and red for L3c. (a) The bvSP in the dataset is classified into five continents based on their isolation regions. The bar graph illustrates the distribution of lineage-specific bvSP across continents, depicted as percentages. (b) The bar graph shows the distribution of bvSP isolated in China by lineage per decade. (c) Geographic distribution of bvSP isolated from China. Doughnut charts in the map show the proportion of lineage types of bvSP collected in the corresponding region, with the total number of isolates in the center.

Figure 2. Phylogenetic tree based on a spatiotemporal Bayesian framework. The phylogenetic tree was constructed based on cgSNPs, with a spatiotemporal Bayesian framework under a relaxed lognormal clock. The evolutionary time was presented by the length of branches and every hundred years as a period. Different colours were used to represent the various lineages of bvSP: fuchsia for L1, orange for L2a, pink for L2b, green for L3b, and red for L3c. The colour strip on the right side represents the ST type, region of isolation, and number of ARGs carried by the corresponding *Salmonella*, respectively.

Figure 3. Genomic characteristics of 45 bvSP newly Isolated from Taishun and Yueqing, Zhejiang Province, China. (a) The phylogenetic tree, constructed using cgSNPs, categorizes the 45 bvSP strains into two distinct lineages (L3c and L2b). The left side of the heatmap displays information on isolation regions, ST types, and sampling times, with various colours indicating different categories as specified on the left side of the heatmap. The right

section of the heatmap presents a detailed matrix showing plasmids, ARGs, and cgSNP distances. The presence of a plasmid or ARGs in an isolate is denoted by gray shading, while absence is indicated by light white. In terms of cgSNP distances, darker circles signify a higher probability of transmission between isolate pairs. (b) The average cgSNP distance between bvSP from Taishun and Yueqing. E404 led to an increase in the mean cgSNP distance of bvSP from Taishun. (c) Invasiveness index of bvSP in Taishun and Yueqing. The results show a higher invasiveness index for bvSP isolated from Taishun, indicating that bvSP isolated from Taishun might have greater invasive capabilities among vulnerable hens.

Figure 4. The ARGs carried by *S.* Gallinarum. (a) The phylogenetic tree was constructed using cgSNPs, revealing three *S.* Gallinarum biovars: bvSG, bvSD, and bvSG. Additionally, *Salmonella* serovar Enteritidis (SE.) is represented by a gray line. Further, bvSP can be subdivided into five lineages: fuchsia (L1), orange (L2a), pink (L2b), green (L3b), and red (L3c). The heatmap on the right indicates the resistome carried by the corresponding *Salmonella*. (b) The dominant resistome types in different regions of China. The y-axis represents the percentage of each dominant resistome. (c) The average number of resistome carried by bvSP is from different regions of China.

Figure 5. The primary source of resistome is carried by distinct mobilome. Different font colours denote various mobilome types. Specifically, orange signifies Integrons, red denotes transposons, blue represents plasmids, and green indicates prophages. A black font is utilized to distinguish the categories of resistome. The connecting line between the resistome and the mobilome represents the potential carrying relationship. (a) The mobilome-carried ARGs among bvSP. (b) The average number of ARGs

carried by the four MGEs in bvSP. (c-e) The mobilome-carried ARGs among bvSP isolated from the eastern, southern, and northern regions of China.

Figure 6. The HGT frequency of the resistome among bvSP isolated from China. (a) Workflow for identification of horizontally transferred ARGs in *Salmonella*. (b) The x-axis represents the resistome of bvSP, while the y-axis represents the corresponding levels of HGT frequency. (c) The overall resistome HGT frequency level of bvSP isolated from various regions of China. (d) The HGT frequency level of specific ARGs carried by bvSP isolated from various regions of China. Deeper colours mean higher HGT frequency. (e) The frequency of horizontal retransmission of the resistome between different regions of China. A higher value indicates more frequent transfer events of resistome between two regions.

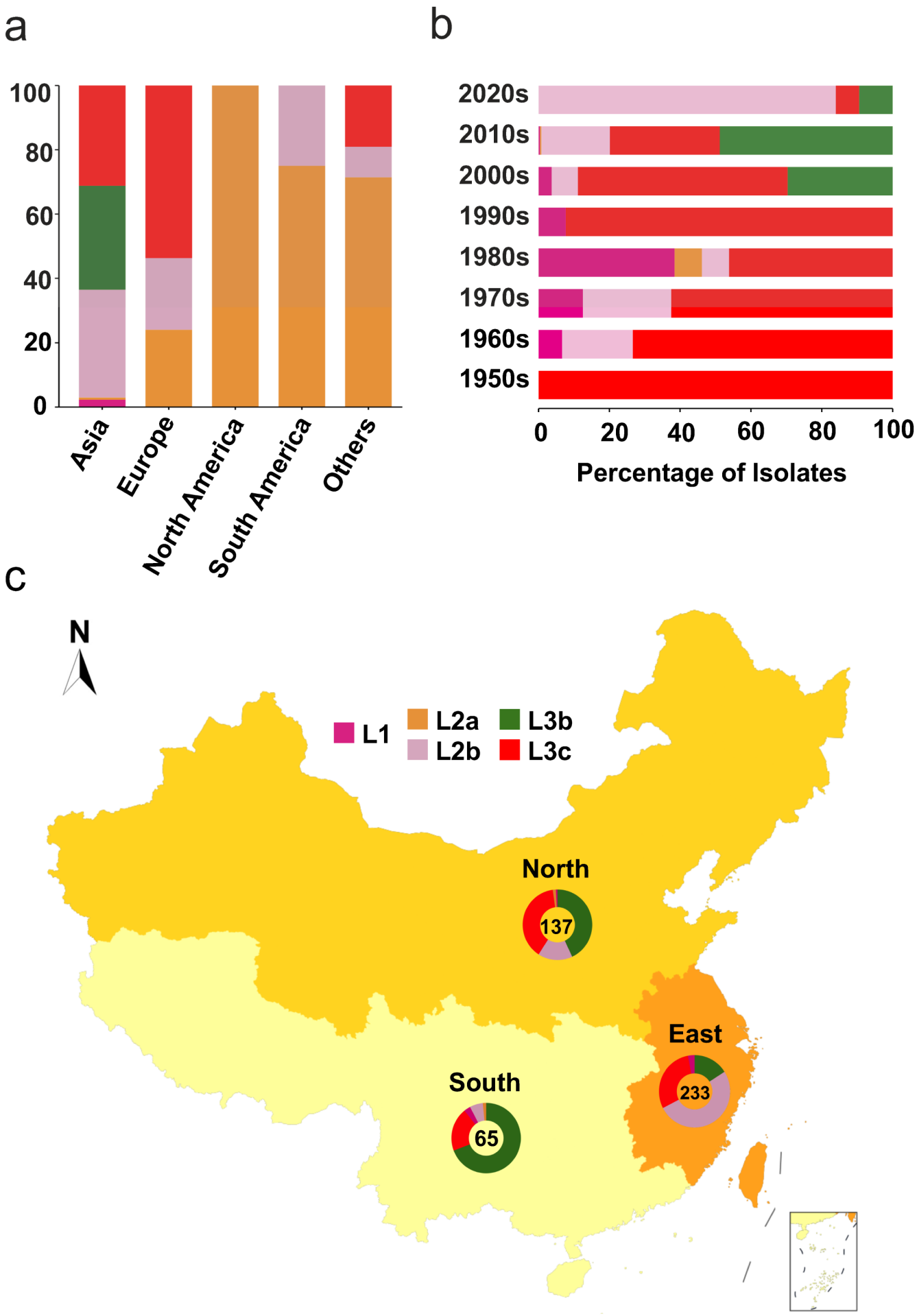
a
100
80
60
40
20
0
Asia
Europe
North America
South America
Others
b
2020s
2010s
2000s
1990s
1980s
1970s
1960s
1950s
0
20
40
60
80
100
Percentage of Isolates
c
N
L1
L2a
L2b
L3b
L3c
North
137
East
233
South
65

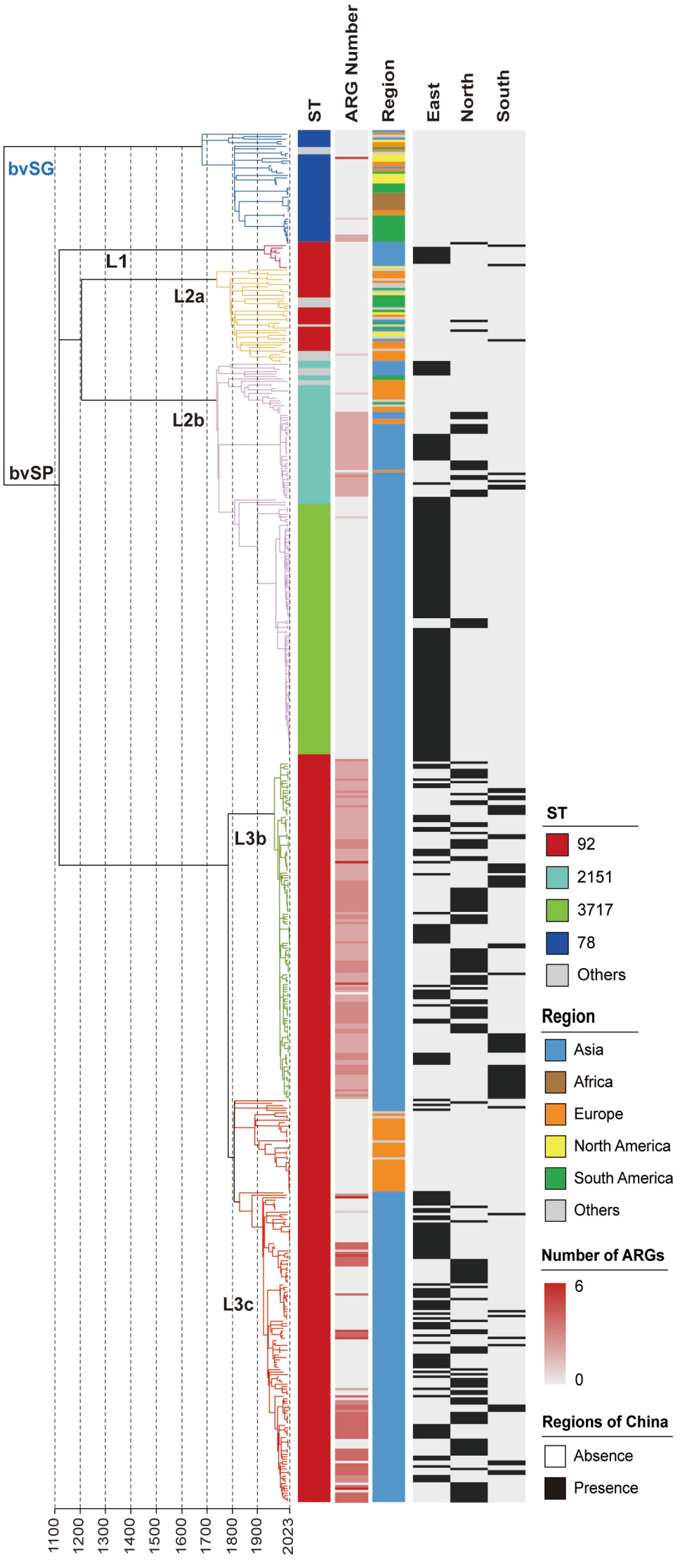
ST
ARG Number
Region
East
North
South
bvSG
L1
L2a
L2b
bvSP
L3b
L3c
1100
1200
1300
1400
1500
1600
1700
1800
1900
2023
ST
92
2151
3717
78
Others
Region
Asia
Africa
Europe
North America
South America
Others
Number of ARGs
6
0
Regions of China
Absence
Presence

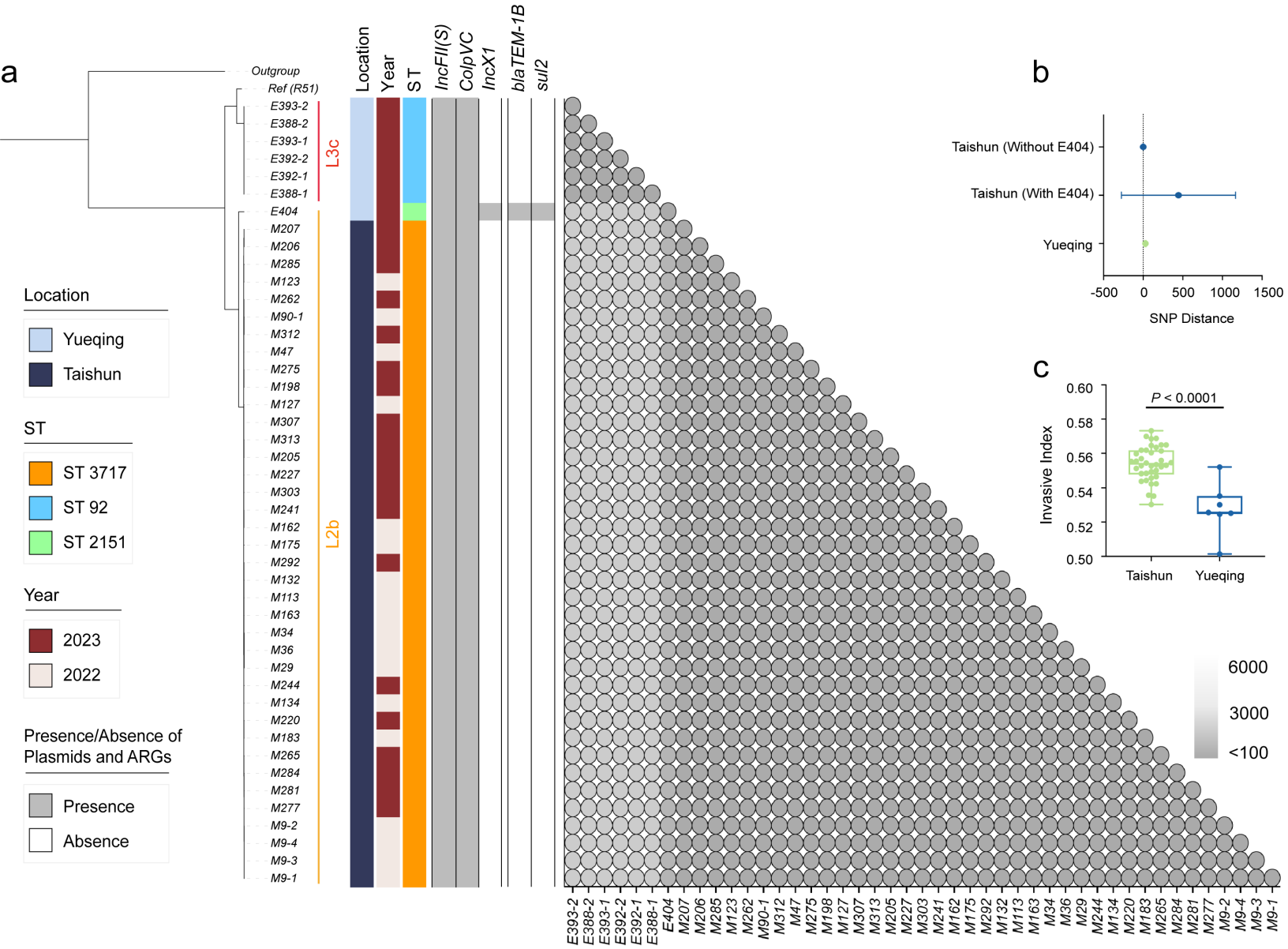
a
Outgroup
Ref (R51)
E393-2
E388-2
E393-1
E392-2
E392-1
E388-1
E404
M207
M206
M285
M123
M262
M90-1
M312
M47
M275
M198
M127
M307
M313
M205
M227
M303
M241
M162
M175
M292
M132
M113
M163
M34
M36
M29
M244
M134
M220
M183
M265
M284
M281
M277
M9-2
M9-4
M9-3
M9-1
L3c
L2b
Location
Year
ST
IncFII(S)
ColpVC
IncX1
blaTEM-1B
sul2
Location
Yueqing
Taishun
ST
ST 3717
ST 92
ST 2151
Year
2023
2022
Presence/Absence of Plasmids and ARGs
Presence
Absence
6000
3000
<100
b
Taishun (Without E404)
Taishun (With E404)
Yueqing
-500
0
500
1000
1500
SNP Distance
c
P < 0.0001
Invasive Index
0.60
0.58
0.56
0.54
0.52
0.50
Taishun
Yueqing

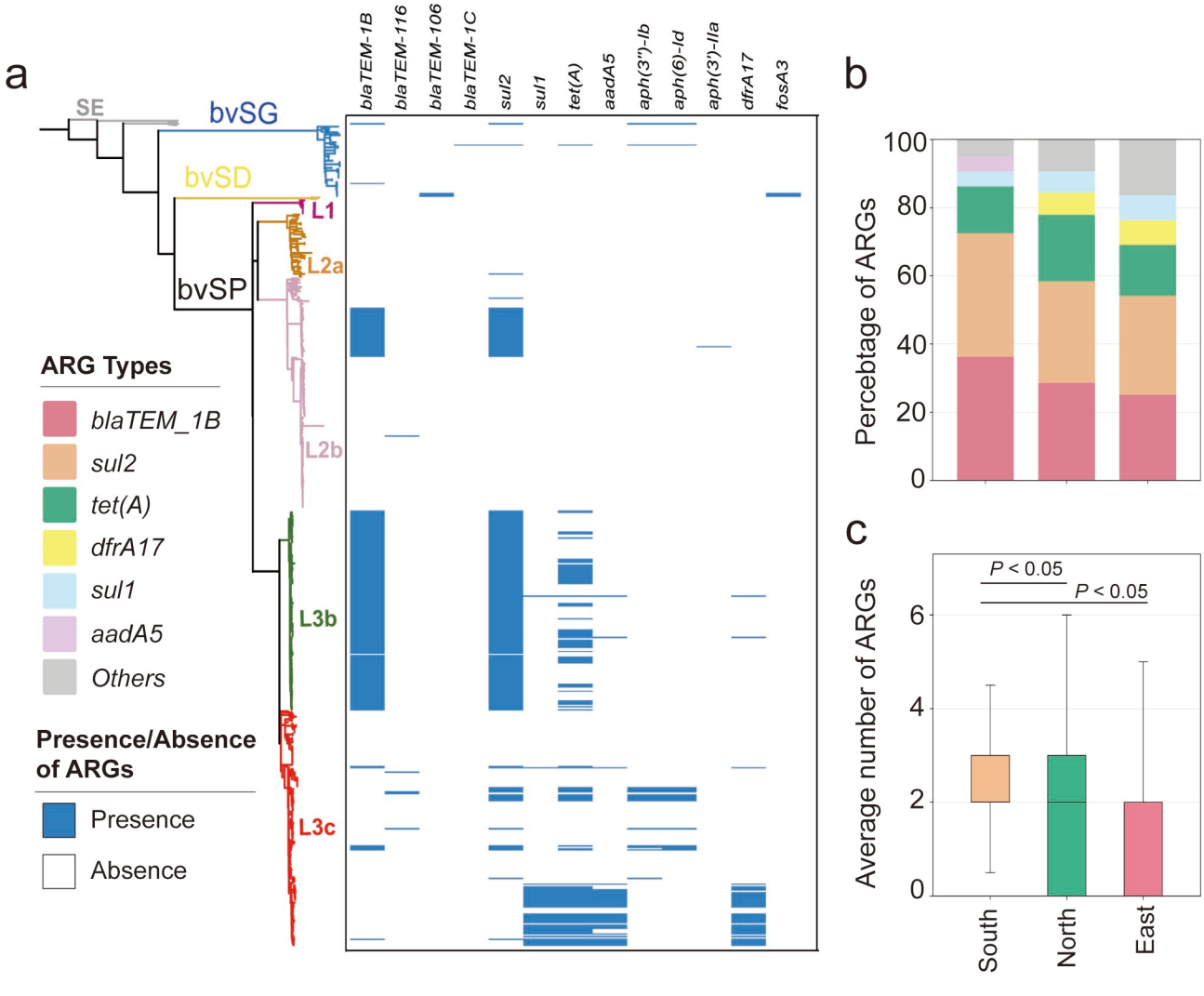
a
SE
bvSG
bvSD
bvSP
L1
L2a
L2b
L3b
L3c
blaTEM-1B
blaTEM-116
blaTEM-106
blaTEM-1C
sul2
sul1
tet(A)
aadA5
aph(3'')-Ib
aph(6)-Id
aph(3')-IIa
dfrA17
fosA3
ARG Types
blaTEM_1B
sul2
tet(A)
dfrA17
sul1
aadA5
Others
Presence/Absence of ARGs
Presence
Absence
b
Percebtage of ARGs
100
80
60
40
20
0
c
Average number of ARGs
P < 0.05
P < 0.05
6
4
2
0
South
North
East

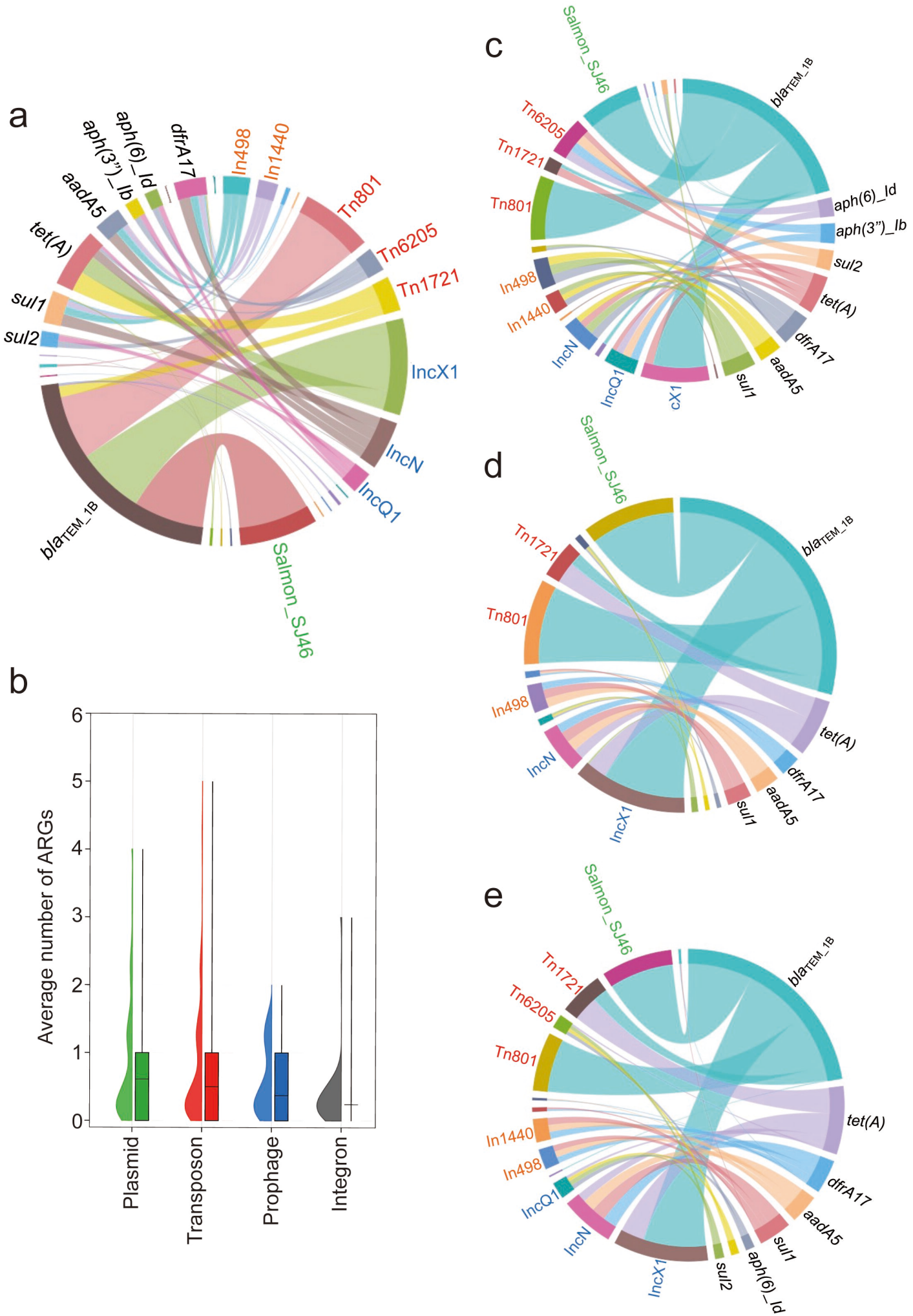
a
Salmon_SJ46
IncQ1
IncN
IncX1
Tn1721
Tn6205
Tn801
In1440
In498
dfrA17
aph(6)_Id
aph(3")_Ib
aadA5
tet(A)
sul1
sul2
blaTEM_1B
b
Average number of ARGs
0
1
2
3
4
5
6
Plasmid
Transposon
Prophage
Integron
c
Salmon_SJ46
Tn6205
Tn1721
Tn801
In498
In1440
IncN
IncQ1
cX1
sul1
aadA5
dfrA17
tet(A)
sul2
aph(3")_Ib
aph(6)_Id
blaTEM_1B
d
Salmon_SJ46
Tn1721
Tn801
In498
IncN
IncX1
sul1
aadA5
dfrA17
tet(A)
blaTEM_1B
e
Salmon_SJ46
Tn1721
Tn6205
Tn801
In1440
In498
IncQ1
IncN
IncX1
sul2
aph(6)_Id
sul1
aadA5
dfrA17
tet(A)
blaTEM_1B

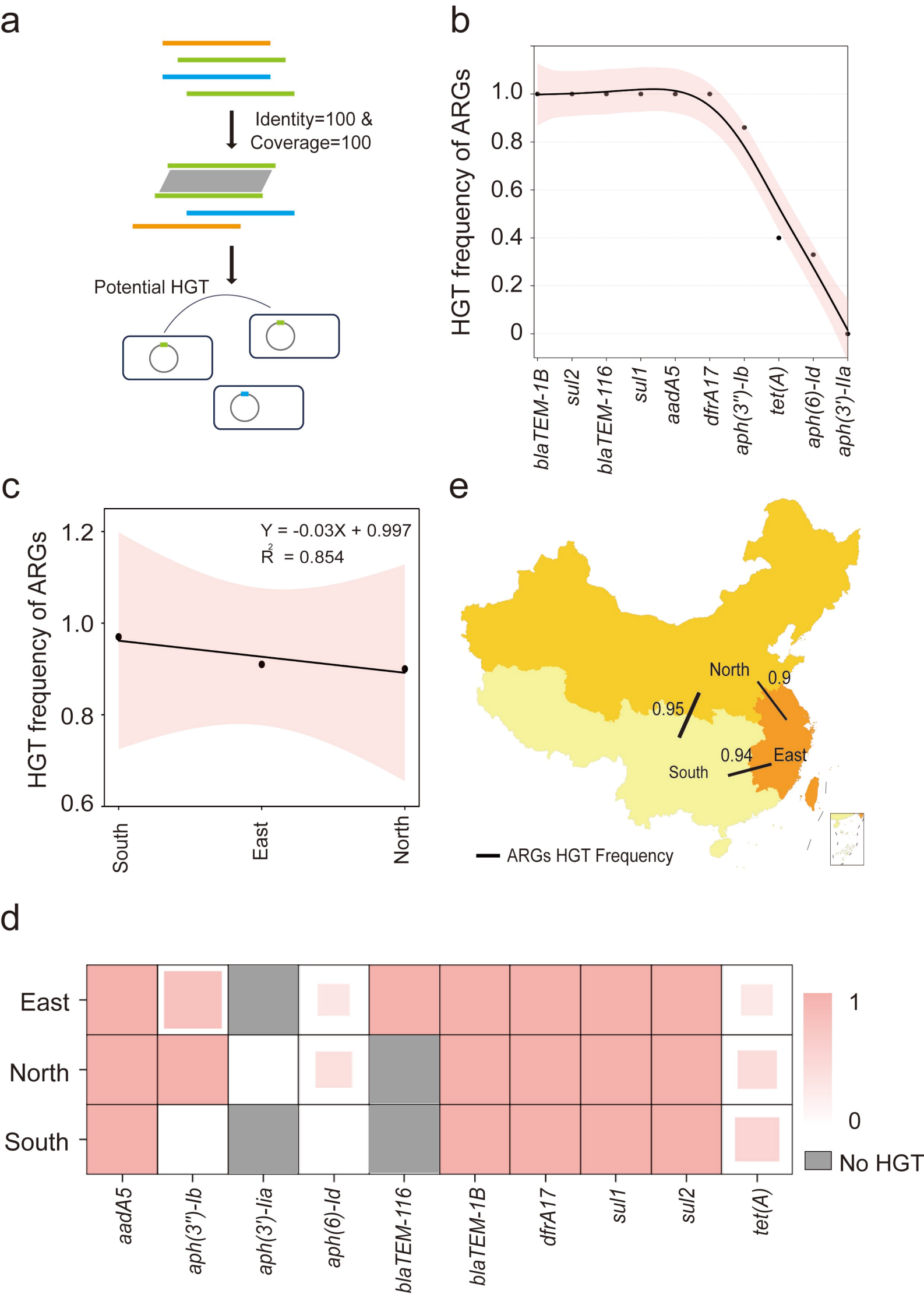
a
Identity=100 &
Coverage=100
Potential HGT
b
HGT frequency of ARGs
1.0
0.8
0.6
0.4
0.2
0
blaTEM-1B
sul2
blaTEM-116
sul1
aadA5
dfrA17
aph(3'')-Ib
tet(A)
aph(6)-Id
aph(3')-IIa
c
Y = -0.03X + 0.997
R2 = 0.854
HGT frequency of ARGs
1.2
1.0
0.8
0.6
South
East
North
e
North
0.9
0.95
0.94
East
South
ARGs HGT Frequency
d
East
North
South
aadA5
aph(3'')-Ib
aph(3')-Iia
aph(6)-Id
blaTEM-116
blaTEM-1B
dfrA17
sul1
sul2
tet(A)
1
0
No HGT